Broadband storage-ring mass and lifetime spectrometry

Yuri A. Litvinov[1,*] and *M. Shahab* Sanjari[1,2]

[1]GSI Helmholtzzentrum für Schwerionenforschung GmbH, Planckstrasse 1, 64291 Darmstadt, Germany
[2]Aachen University of Applied Sciences, Bayernallee 11, 52066 Aachen, Germany

Abstract. The mass and half-life of a nucleus are its basic properties which reflect its structure and decay properties. These data are among the most important nuclear physics inputs to astrophysical nucleosynthesis modelling. Tremendous experimental efforts are carried out to obtain yet unknown quantities, which are as a rule belong to short-lived nuclei far away from stability. Storage ring mass spectrometry is a technique ideally suited for addressing many different nuclear species at the same time. In the last few years it went through major developments regarding nuclear mass determinations, thereby boosting its efficiency, sensitivity and precision. A non-destructive detection capability is being presently implemented aiming at simultaneous mass, lifetime and decay branching measurements. Recent developments and future perspectives are briefly discussed.

1 Introduction

Atomic nuclei are composed of two kinds of quantum particles, protons and neutrons, which are kept together by a highly complicated nuclear force. This force defines the structure of nuclei, their shapes and moments, decay properties and correlations among nucleons [1]. Total energies, $E(Z,N)$, of various nuclei with different numbers of protons, Z, and neutrons, N, spanning over the entire chart of the nuclides, contain answers on the result of this nuclear interaction at work. $E(Z,N)$, or the rest mass, $m(Z,N)$, is directly connected to the binding energy, $B(Z,N)$, via:

$$m(Z,N) = E(Z,N)/c^2 = Z \cdot m_p + N \cdot m_n - B(Z,N), \quad (1)$$

where m_p, m_n are the rest masses of proton and neutron, respectively. The mass of the corresponding atom can be obtained by adding the masses of electrons and removing their binding energies [2]. Nuclear masses plotted on a nuclear chart form the *nuclear mass surface*. This surface is in general very smooth and changes in nuclear structure appear on it as irregularities [3].

Masses of the nuclei define whether and which radioactive transformation between them is possible. Of particular interest are weak decays, which dominate throughout the nuclear chart. Both quantities, masses and beta-decay lifetimes, are required in nuclear astrophysics, where the former ones define the pathways of nucleosynthesis processes on the nuclear chart and the latter ones affect the accumulated element abundances [4, 5].

In the past 100 years masses of about 2550 nuclei have been measured [6], whereas about 7000 bound nuclei are expected to exist [7]. These extensive data are employed to benchmark nuclear theories [8, 9]. However, their predictive powers are still insufficient for many applications in nuclear structure and astrophysics. Therefore, the measurements of still unknown masses is highly desired, which will again be used to further constrain theory. Taken their importance, mass measurements belong to research programs at basically all present and planned radioactive-ion beam facilities. Mass spectrometry methods are exhaustively reviewed in literature [10–17].

The experimental masses are evaluated in the Atomic Mass Evaluation (AME) [6], which also contains short-range extrapolations to yet unmeasured nuclides. The masses and half-lives are conveniently presented in the NUBASE database [18]. By inspecting NUBASE, one can notice that half-lives are typically known for more exotic nuclei than those with measured masses, which can be explained by the fact that many particles are required in modern mass spectrometry methods. Measurements of yet unknown masses are extremely challenging. To significantly advance further, a technique is required which would be capable to determine precisely the mass from ideally a single particle. At the same time, such a technique needs to be very fast since the characteristic half-lives of the nuclei of interest are well below one second. Furthermore, a dream would turn into reality, if the lifetime determination is conducted at the same time. In this context, storage ring mass spectrometry is a promising approach.

There are presently three heavy-ion storage rings coupled to radioactive ion-beam facilities [16, 17]. The facility at GSI Helmholtz Center in Germany comprises heavy-ion synchrotron SIS, projectile fragment separator FRS and the experimental storage ring ESR [19, 20]. At the Institute of Modern Physics in China, the experimental cooler-storage ring CSRe is connected to the synchrotron CSRm via the fragment separator RIBLL2 [21, 22]. Quasi-DC beams from a high-power cyclotron are employed at RIKEN Nishina Center in Japan, where the rare-ion storage ring R3 is placed behind the high-acceptance separator Big-RIPS [23]. At all these facili-

*e-mail: y.litvinov@gsi.de

ties, the secondary ions of interest are produced at high energies of a few hundreds of AMeV, utilizing mainly the projectile fragmentation or fission nuclear reactions [24]. At these energies, fragments are as a rule fully-ionized or have just a very few bound electrons [25]. At the ESR and CSRe, all fragments fitting into the acceptance of the machines are transported, injected and stored. The peculiarity of the R3 is that the injection of individual pre-identified particles is implemented [26].

This short contribution does not aim at providing details of specific facilities and/or experiments. Instead it focuses on recent developments of the storage ring mass spectrometry as well as on somewhat speculative future perspectives.

2 Storage ring mass spectrometry

Motion of a relativistic particle with mass-over-charge ratio m/q and velocity v in a heavy-ion storage ring is analogous to the one in a synchrotron and is given by [27]:

$$\frac{\Delta f}{f} = \eta \frac{\Delta p}{p}, \tag{2}$$

where f and $p = mv\gamma$ are, respectively, the revolution frequency and momentum of the particle. The parameter η is defined as:

$$\eta = \frac{1}{\gamma_t^2} - \alpha_p = \frac{1}{\gamma^2} - \frac{1}{\gamma_t^2}, \tag{3}$$

with γ and γ_t being the relativistic Lorentz factor corresponding to particle energy in general and at a specific value known as *transition energy*, which is defined by the ion optics of the ring. In accelerator physics, $\alpha_p = 1/\gamma_t^2$ is termed *momentum compaction factor*. It describes the variation of the orbit length $\Delta C/C$ corresponding to a change of the magnetic rigidity $\Delta B\rho/B\rho$, with $B\rho = mv\gamma/q$. In order to enable acceleration or deceleration in a synchrotron, the condition $\eta \neq 0$ or $\gamma_t \neq \gamma$ must hold. However, beam can be stored also for $\eta = 0$ or $\gamma_t = \gamma$. These optical settings are called *standard* and *isochronous* modes, respectively [28].

Assuming a closed trajectory, the revolution frequency is given as $f = v/C$. By combining the above equations, the basic formula for *storage ring mass spectrometry* can be derived [20]:

$$\frac{\Delta f}{f} = -\frac{\Delta T}{T} = -\frac{1}{\gamma_t}\frac{\Delta(m/q)}{m/q} + \frac{\Delta v}{v}\left(1 - \frac{\gamma^2}{\gamma_t^2}\right), \tag{4}$$

where T is the revolution time.

According to Eq. (4), the revolution frequencies of the stored particles reflect their mass-over-charge ratios, provided the second term on the right hand side vanishes. The revolution frequency scale is calibrated utilizing numerous different nuclear species with experimentally known masses that are transmitted and injected in the same machine setting. The remaining challenge is that the secondary particles are produced in a nuclear reaction and their velocity spread $\Delta v/v$ in the present context is huge [25].

In the standard mode, $\Delta v/v$ is reduced by cooling the beam utilizing stochastic and/or electron cooling [29, 30]. For low-intensity fragment beams, small velocity spreads of $\Delta v/v \approx 10^{-7}$ can be achieved. However, the cooling process requires a few seconds to complete. Therefore, in spite of very successful usage in the past [31–36], this approach has a limited applicability for mass measurements of short-lived nuclei. Nevertheless, beam cooling will remain inevitable for investigations of exotic decay modes [37, 38].

In the isochronous mode, ion optics of the ring is changed so that the transition energy can be matched to the energy of the particle. In this mode, the differences in particle momenta for a given particle species are compensated by the lengths of their orbits, leading to the same revolution frequencies [39, 40]. The time consuming cooling is not needed and, apart from the negligible flight time from the production target until the injection into the ring, the measurement can start without any further delay. Therefore, *isochronous mass spectrometry* (IMS) is the technique of choice for short lived nuclei.

To be stored, $B\rho$ of the ion must match the range of $B\rho$ values accepted by the machine. Due to the broad momentum distributions, particles with very different m/q can be transmitted. On the one hand, this enables us to cover a large ($\Delta(m/q)/(m/q)$ of several percent) region of the nuclidic chart in a single setting [41, 42]. On the other hand, the required condition $\gamma = \gamma_t$ is not fulfilled for all ions. According to Eq. (4), the spread $\Delta f/f$ or $\Delta T/T$ increases with γ deviating from the fixed γ_t. Black squares in Fig. 1 illustrate the growth of revolution time widths, σ_T, as a function of m/q for ^{58}Ni projectile fragments measured in the CSRe [43, 44]. The range of m/q values corresponding to the smallest peak widths of $\sigma_T \approx 2$ ps is termed *isochronous window*. The nuclei outside of the isochronous window are typically disregarded in data analyses [41].

3 Revolution frequency determination

There are two ways to measure revolution frequencies or, equivalently, revolution times of the stored ions.

The first one employs a very thin foil inserted into the ring aperture. When a relativistic ion punches through the foil, secondary electrons are released on both sides of the foil. These electrons are guided by perpendicularly arranged electrostatic and weak magnetic fields to fast avalanche detectors, typically micro-channel plates. The signal from the anode is continuously sampled with high rate, reaching nowadays 50 giga-samples per second. As a result, each particle causes a train of repeating signals, which are unambiguously identified in the offline analysis. Procedures to extract mean revolution times take into account variations due to field inhomogeneities, energy losses in the foil, etc. The number of secondary electrons depends on the charge of the ion, which can be utilized as an additional identification criterion [47, 48].

Several implementations of such time-of-flight detectors have been in use at all three facilities in operation [49–53]. Also new-generation detectors are being prepared and

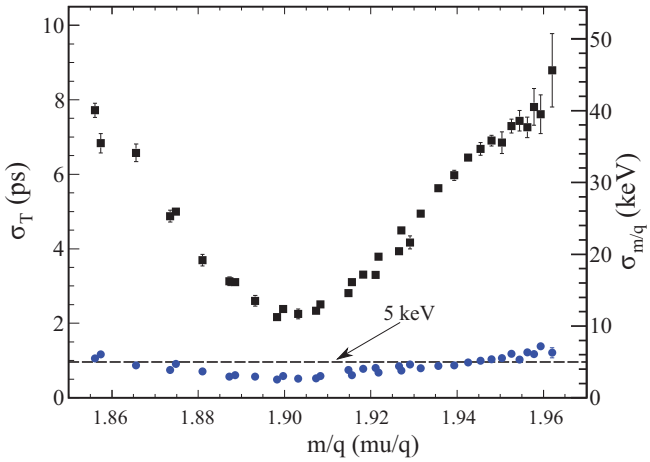

Figure 1. Standard deviations of the revolution-time peaks (left scale) for ^{58}Ni projectile fragments measured in the CSRe. The widths obtained with and without using the information on particle velocities are shown, respectively, with blue circles and black squares. The right scale provides the corresponding absolute accuracy of mass-over-charge ratios. Taken from [43, 44].

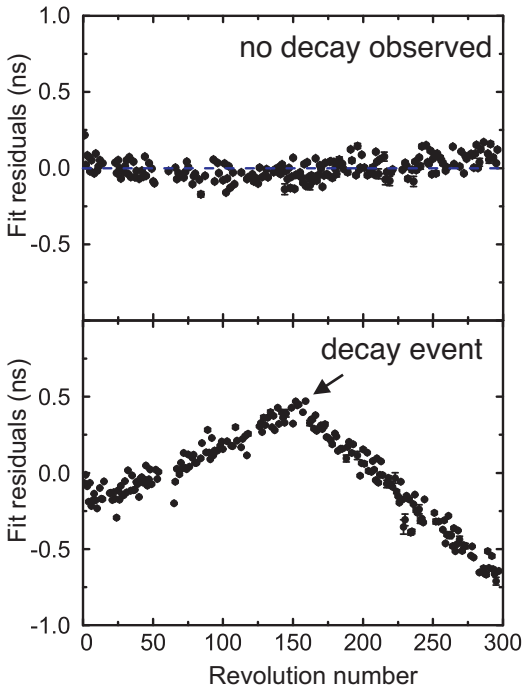

Figure 2. Residuals to the fits of timing signals for two ^{94m}Ru^{44+} ions measured by a time-of-flight detector in the CSRe. No changes in the slope, which would indicate a change of the m/q value, are seen for the ion in the top panel. A clear kink is observed in the lower panel. This kink manifests the de-excitation of ^{94m}Ru^{44+} isomer to the corresponding ground state ^{94g}Ru^{44+}. Modified from [56].

are optimized for the future storage rings [54]. The advantage of this approach is that only a few ten turns are sufficient to determine the revolution time, where one revolution takes merely a fraction of microsecond. An obvious disadvantage is that the overall method is destructive. Particles are lost after a few hundred revolutions. Therefore, in the context of the present discussion, no simultaneous lifetime measurements is possible. Exceptions are microsecond isomers which decay within these few hundred revolutions [55, 56], as illustrated in Fig. 2.

The second method employs Schottky detectors. Revolving particles periodically pass by these detectors. Highly charged particles induce an equal amount of charge on the conductive surface of the vacuum pipe, and hence also on the surface of the detector electrodes. Over the years, detectors have evolved from capacitive copper plate electrodes to sophisticated cavity-based resonators [57]. The Fourier analysis of the amplified output from the detector yields the noise power spectrum or *Schottky frequency spectrum*. Typically, higher harmonics of the ion revolution frequencies are analyzed, reaching $h \approx 200$ in the latest detector in the ESR [58]. The main advantage of these devices is that the detection of revolution frequencies is non-destructive. Whereas the frequencies in the Schottky spectrum are used for mass determinations, the amplitudes of the peaks are proportional to the corresponding numbers of the stored ions [59, 60]. By monitoring the development of peak areas in time, decay constants can be obtained [61, 62]. Furthermore, since the storage ring has a large acceptance, the decay daughter ions often stay in the machine. In such cases, combined analysis of the decrease of the peak area of the parent ions and the increase of the area(s) of the daughter-ion species enables one to establish also the branching ratios [63–66]. In addition, the detectors have no dynamic range limitations and are capable of simultaneously addressing single stored ions and milliampere beams.

Until very recently, Schottky-noise detectors were employed in experiments in standard operation mode with cooled ions. This technique is broadly known as time-resolved *Schottky mass spectrometry* (SMS) [67]. The

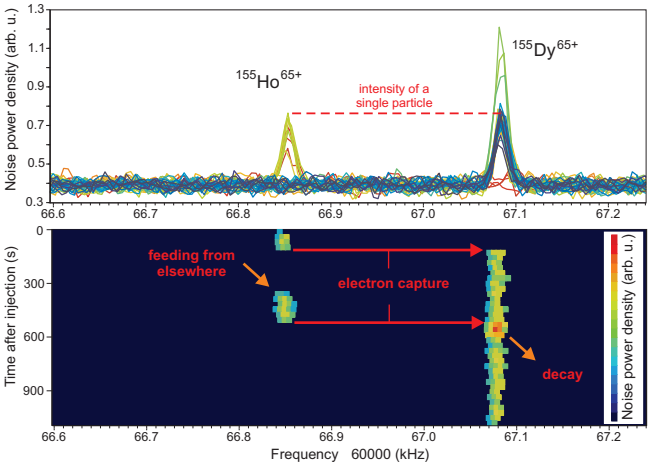

Figure 3. Time-resolved Schottky frequency spectra of $A = 165$ isobars produced in fragmentation of ^{209}Bi measured in the ESR. The time resolution is 30 s. Displayed is the 30$^{\text{th}}$ harmonic of the revolution frequency. Top panel illustrates individual spectra which indicate the constancy of the single-particle areas. The bottom panel shows the development of peak areas in time. See labels in the figure for more details. Redrawn from [67].

first generations of Schottky detectors required integration over several ten seconds to observe revolution frequencies of single ions. One such example is shown in Fig. 3. However, the detectors based on resonant cavities allowed for a considerable increase of time resolution. Presently, several milliseconds are sufficient for the frequency measurement [68, 69]. With this development, a straightforward next step is to employ such detectors in the isochronous mode. The first application of such combined time-resolved Schottky plus isochronous mass spectrometry (S+IMS) was done in the CSRe where half-lives of fully ionized $^{49}Cr^{24+}$ and $^{53}Fe^{26+}$ ions were measured [70].

The S+IMS technique has successfully been applied in the ESR to measure two-photon de-excitation of the first 0^+ state in ^{72}Ge [71]. The corresponding half-life is just a few ten milliseconds which confirms the power of the method. The data analysis is in its final stage and the results will be reported soon.

4 Velocity determination

The limitation set by the isochronous window severely reduces the efficiency of the method, where only a part of measured data is used. It has been suggested in [72] that an additional information on $B\rho$ or v of each stored ion is needed to expand the isochronous window ideally over the entire ring acceptance. In a test experiment in the ESR, $B\rho$ was defined by mechanical slits in the FRS to $\Delta B\rho/(B\rho) \approx 1.5 \times 10^{-4}$ [73]. Measurements were conducted employing a time-of-flight detector. A part of the revolution time spectrum in a region far away from the isochronous window is illustrated in Fig. 4. By applying this so-called *Bρ-tagging* method, improvement of the resolving power by up to a factor of eight was reported, though it is evident that the transmission efficiency is dramatically reduced.

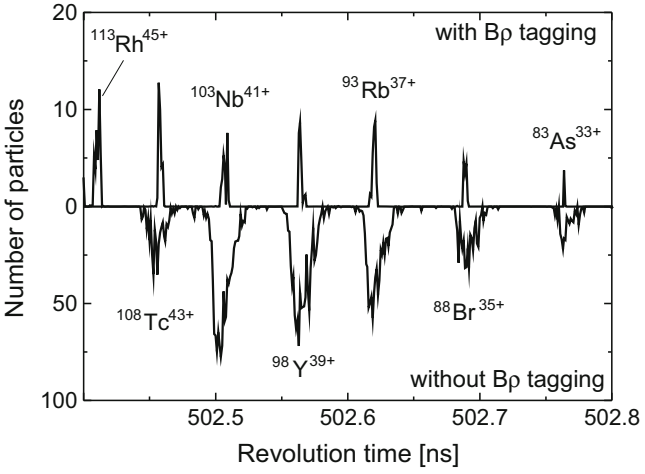

Figure 4. Parts of the revolution time spectra of ^{238}U fission fragments measured in the ESR by applying a time-of-flight detector. The shown region is far away from the isochronous window. Upper panel: The magnetic rigidities were limited in the FRS to $\Delta B\rho/(B\rho) \approx 1.5 \times 10^{-4}$. Lower panel: No cuts have been applied to the transmitted beam. Taken from [73].

The determination of $B\rho$ or v for every ion without limiting the transmission became the major quest of the storage ring mass spectrometry. At the R3, as mentioned earlier, the necessary identification of every ion includes the measurement of its time-of-flight in the Big-RIPS, which delivers information on the ion velocity prior to its injection into the ring [74]. At the CSRe, two identical time-of-flight detectors were installed in a straight section [75, 76]. Two trains of timing signals are obtained from these detectors, which provides information v and in turn on C and $B\rho$ for every ion [77]. Since the ions with the same $B\rho$ must have the same mean C, a very powerful analysis has been developed which enabled correction for non-isochronicity throughout the entire CSRe acceptance [43]. The improvement of the resolving power can be followed through the reduced peak widths shown with blue circles in Fig. 1. The dashed line indicated the absolute $m/q = 5$ keV limit. This means that by detecting just a single ion, its m/q value can be determined with this mass uncertainty, which is remarkable. This has been demonstrated through mass measurements of exotic ^{78}Kr projectile fragments in the CSRe. Only 4 particles were observed for ^{70}Kr and for ^{75}Sr, corresponding to the rate of two ions per week [78, 79]. This technique was named $B\rho$-defined IMS or just $B\rho$-IMS. By combining this sensitivity, speed of the measurement, efficiency and achieved mass precision, $B\rho$-IMS became one of the most powerful mass measurement methods.

However, the destructive time-of-flight detectors do not allow for addressing lifetimes and this remains an unsolved challenge. The pursued solution is to employ position sensitive Schottky cavities installed in a dispersive location of the ring [80–82]. The center of the cavity is placed at an offset to the beam pipe. Two cavities for two transverse directions are needed. The amplification gradient falls from the middle of the cavity towards its edge. Particles of the same charge passing the cavity at different locations will thus produce signals with different amplitudes. A high resolution Schottky cavity will be used for high precision frequency measurement which in turn will provide information on the charge of every particle. Combined information will be used to determine $B\rho$ of every ion. The prototype cavities for the proof-of-principle experiments are being constructed for the ESR and the R3 [83]. Dependent on the position sensitivity, a similar resolving power as shown in Fig. 1 could be envisaged.

5 Outlook

The mass measurement programs at the present ESR, CSRe and R3 storage rings have delivered important results, see e.g. [84–96]. They will continue in the future and even further expanded at the next-generation facilities FAIR, Germany and HIAF, China. The collector ring (CR) at FAIR [97] and spectroscopy ring (SRing) at HIAF [98] have been dedicatedly designed for IMS experiments. In comparison to IMS with a single time-of-flight detector and $B\rho$-tagging option, the $B\rho$-IMS technique has proven its superior efficiency. Therefore, both rings will have setups with two high-aperture time-of-flight detectors as required by the $B\rho$-IMS.

Implementation of longitudinal-sensitive Schottky cavities in the IMS enabled the S+IMS, which has been applied to half-life determinations. Further improvement of the time resolution of the S+IMS will be possible with higher quality cavities, though the price to pay is the lower bandwidth. Hence, several cavities tuned at different overlapping frequency ranges will be needed to cover the ring acceptance [99]. The most promising development is related to cavities with transverse-sensitivity. The non-destructive position determination will boost the mass resolving power. If successful, this will enable non-destructive mass measurements of short-lived nuclides. Simultaneously, the information on their lifetimes will be acquired as well.

Employing multiple Schottky cavities is a challenging task extending beyond the design on the detectors. Major advances in data handling and data analysis methods have been made in recent years, contributing to an unprecedented understanding of the devices themselves, but also allowing larger amounts of data to be processed for increased accuracy. For offline analysis, software frameworks have been developed to run on larger computer clusters to process large amounts of raw data [100]. The operation of Schottky detectors requires dedicated data acquisition systems. Data from multiple narrow-band and broadband Schottky detectors acquired by separate DAQ systems can be combined for online and offline analysis in order to combine the advantages of narrow-band data acquisition with a super-wide spectrum covering multiple revolution harmonics. To this end, open source and open hardware DAQ systems based on Software Defined Radio SDR for continuous and distributed data acquisition are planned [101].

In conclusion, taken that in the IMS: (i) a big region of the nuclidic chart is addressed at the same time, (ii) a single ion is sufficient for a successful measurement, and (iii) the time resolution is in the ten millisecond range, storage ring mass and lifetime spectrometry has the potential to deliver properties of nuclides in ground and isomeric states, which are simply inaccessible by other techniques.

Acknowledgements

This contribution would not be possible without successful collaboration with colleagues working at the ESR, CSRe and R3. This research received support from the European Research Council (ERC) under the EU Horizon 2020 research and innovation programme (ERC-CoG "ASTRUm"), and the State of Hesse within the Research Cluster ELEMENTS (Project ID 500/10.006).

References

[1] A. Bohr and B.R. Mottelson, *Nuclear Structure*, World Scientific Publ., Singapore, 1998.
[2] G. C. Rodrigues, *et al.*, At. Data Nucl. Data Tab. **86**, 117–233 (2004).
[3] Yu. N. Novikov, *et al.*, Nucl. Phys. A **697**, 92–106 (2002).
[4] E. M. Burbidge, *et al.*, Rev. Mod. Phys. **29**, 547–650 (1957).
[5] J. J. Cowan, *et al.*, Rev. Mod. Phys. **93**, 015002 (2021).
[6] W. J. Huang, *et al.*, Chin. Phys. C **45**, 030002 (2021).
[7] J. Erler, *et al.*, Nature **486**, 509 (2012).
[8] A. Sobiczewski, *et al.*, Phys. Rev. C **89**, 024311 (2014).
[9] A. Sobiczewski, *et al.*, At. Data Nucl. Data Tables **119**, 1–32 (2018).
[10] D. Lunney *et al.*, Rev. Mod. Phys. **75**, 1021–1082 (2003).
[11] K. Blaum, Phys. Rep. **425**, 1–78 (2006).
[12] F. Bosch, *et al.*, Int. J. Mass Spectr. **251**, 212–219 (2006).
[13] F. Bosch, *et al.*, Int. J. Mass Spectr. **349-350**, 151–161 (2013).
[14] Y. Litvinov, *et al.*, Nucl. Instr. Meth. B **317**, 603–616 (2013).
[15] T. Eronen, *et al.*, Prog. Part. Nucl. Phys. **91**, 259–293 (2016).
[16] Y. H. Zhang, *et al.*, Phys. Scripta **91**, 073002 (2016).
[17] T. Yamaguchi, *et al.*, Prog. Part. Nucl. Phys. **120**, 103882 (2021).
[18] F. G. Kondev, *et al.*, Chin. Phys. C **45**, 030001 (2021).
[19] H. Geissel, *et al.*, Phys. Rev. Lett. **68**, 3412-3415 (1992).
[20] B. Franzke, H. Geissel and G. Münzenberg, Mass Spectr. Rev. **27**, 428–469 (2008).
[21] J. Xia, *et al.*, Nucl. Instr. Meth. A **488**, 11–25 (2002).
[22] M. Z. Sun, *et al.*, Front. Phys. **13**, 132112 (2018).
[23] A. Ozawa, *et al.*, Prog. Theor. Exp. Phys. **2012**, 03C009 (2012).
[24] C. A. Bertulani and P. Danielewicz, *Introduction to Nuclear Reactions*, CRC Press, Boca Raton, 2021.
[25] H. Geissel, G. Münzenberg and K. Riisager, Ann. Rev. Nucl. Part. Sci. **45**, 163-203 (1995).
[26] T. Yamaguchi, *et al.*, Int. J. Mass Spectr. **349-350**, 240–246 (2013).
[27] F. Hinterberger, *Physik der Teilchenbeschleuniger und Ionenoptik*, Springer-Verlag, Berlin, Heidelberg, 2008.
[28] M. Steck and Yu. A. Litvinov, Prog. Part. Nucl. Phys. **115**, 103811 (2020).
[29] H. Geissel, *et al.*, Nucl. Phys. A **746**, 150–155 (2004).
[30] H. Geissel, *et al.*, Eur. J. Special Topics **150**, 109–115 (2007).
[31] T. Radon *et al.*, Phys. Rev. Lett. **78**, 4701–4704 (1997).
[32] T. Radon, *et al.*, Nucl. Phys. A **677**, 75-99 (2000).
[33] Y. Litvinov, *et al.*, Nucl. Phys. A **756**, 3–38 (2005).
[34] L. Chen *et al.*, Phys. Rev. Lett. **102**, 122503 (2009).
[35] L. Chen *et al.*, Phys. Lett. B **691**, 234–237 (2010).
[36] D. Shubina, *et al.*, Phys. Rev. C **88**, 024310 (2003).

[37] Y. Litvinov, *et al.*, Rep. Prog. Phys. **74**, 016301 (2011).
[38] F. Bosch, *et al.*, Prog. Part. Nucl. Phys. **73**, 84–140 (2013).
[39] M. Hausmann, *et al.*, Nucl. Instr. Meth. A **446**, 569–580 (2000).
[40] M. Hausmann, *et al.*, Hyperf. Interactions **132**, 289–295 (2001).
[41] B. Sun, *et al.*, Nucl. Phys. A **812**, 1–12 (2008).
[42] X. Tu, *et al.*, Nucl. Instr. Meth. A **654**, 213–218 (2011).
[43] M. Wang *et al.*, Phys. Rev. C **106**, L051301 (2022).
[44] M. Zhang *et al.*, Eur. Phys. J. A **59**, 27 (2023).
[45] M. Zhang *et al.*, Nucl. Instr. Meth. A **1027**, 166329 (2022).
[46] Y. M. Xing *et al.*, Phys. Rev. C **107**, 014304 (2023).
[47] P. Shuai, *et al.*, Phys. Lett. B **735**, 327–331 (2014).
[48] X. Zhou, *et al.*, Nucl. Sci. Techniq. **32**, 37 (2021).
[49] J. Trötscher *et al.*, Nucl. Instr. Meth. B **70**, 455–458 (1992).
[50] B. Mei *et al.*, Nucl. Instr. Meth. A **624**, 109–113 (2009).
[51] W. Zhang *et al.*, Nucl. Instr. Meth. A **755**, 38–43 (2014).
[52] W. Zhang *et al.*, Nucl. Instr. Meth. A **756**, 1–5 (2014).
[53] D. Nagae *et al.*, Nucl. Instr. Meth. A **986**, 164713 (2021).
[54] N. Kuzminchuk-Feuerstein *et al.*, Nucl. Instr. Meth. A **821**, 160–168 (2016).
[55] B. Sun *et al.*, Phys. Lett. B **688**, 294–297 (2010).
[56] Q. Zeng *et al.*, Phys. Rev. C **96**, 031303 (2017).
[57] F. Nolden, *et al.*, Nucl. Instr. Meth. A **659**, 69–77 (2011).
[58] M. S. Sanjari, *et al.*, Rev. Sci. Instr. **91**, 083303 (2020).
[59] H. Irnich, *et al.*, Phys. Rev. Lett. **75**, 4182–4185 (1995).
[60] Y. Litvinov, *et al.*, Phys. Lett. B **573**, 80–85 (2003).
[61] Y. Litvinov, *et al.*, Phys. Lett. B **664**, 162–168 (2008).
[62] D. Atanasov, *et al.*, J. Phys. B **48**, 144024 (2015).
[63] T. Ohtsubo, *et al.*, Phys. Rev. Lett. **95**, 052501 (2005).
[64] Y. Litvinov, *et al.*, Phys. Rev. Lett. **99**, 262501 (2007).
[65] N. Winckler, *et al.*, Phys. Lett. B **679**, 36–40 (2009).
[66] D. R. Atanasov, *et al.*, Eur. Phys. J. A **48**, 22 (2012).
[67] Y. Litvinov, *et al.*, Nucl. Phys. A **734**, 473-476 (2004).
[68] P. Kienle, *et al.*, Phys. Lett. B **726**, 638–645 (2013).
[69] F. Ozturk, *et al.*, Phys. Lett. B **797**, 134800 (2019).
[70] X. L. Tu, *et al.*, Phys. Rev. C **97**, 014321 (2018).
[71] W. Korten, *et al.*, Proposal, GSI Program Advisory Committee (2022).
[72] H. Geissel, *et al.*, J. Phys. G **31**, S1779–S1783 (2005).
[73] H. Geissel, *et al.*, Hyperf. Interactions **173**, 49–54 (2006).
[74] H. F. Li, *et al.*, Phys. Rev. Lett. **128**, 152701 (2022).
[75] P. Shuai, *et al.*, Nucl. Instr. Meth. B **376**, 311–315 (2016).
[76] X. L. Yan, *et al.*, Nucl. Instr. Meth. A **931**, 52–59 (2019).
[77] X. Zhou, *et al.*, Phys. Rev. Accel. Beams **24**, 042802 (2021).
[78] X. Zhou, *et al.*, Nat. Phys., in press (2023).
[79] M. Wang, *et al.*, Phys. Rev. Lett., in press (2023).
[80] M. S. Sanjari, *et al.*, Phys. Scripta **T166**, 014060 (2015).
[81] X. Chen, *et al.*, Hyperf. Interactions **235**, 51–59 (2015).
[82] X. Chen, *et al.*, Nucl. Instr. Meth. A **826**, 39–47 (2016).
[83] D. Dmytriiev, *et al.*, Nucl. Instr. Meth. B **463**, 320–323 (2020).
[84] J. Stadlmann, *et al.*, Phys. Lett. B **586**, 27–33 (2004).
[85] Y. Litvinov, *et al.*, Phys. Rev. Lett. **95**, 042501 (2005).
[86] M. W. Reed, *et al.*, Phys. Rev. Lett. **105**, 172501 (2010).
[87] X. Tu, *et al.*, Phys. Rev. Lett. **106**, 112501 (2011).
[88] Y. Zhang, *et al.*, Phys. Rev. Lett. **109**, 102501 (2012).
[89] X. L. Yan, *et al.*, Astroph. J. Lett. **766**, L8 (2013).
[90] L. Chen, *et al.*, Phys. Rev. Lett. **110**, 122502 (2013).
[91] X. Xu, *et al.*, Phys. Rev. Lett. **117**, 182503 (2016).
[92] R. Knöbel, *et al.*, Eur. Phys. J. A **52**, 138 (2016).
[93] R. Knöbel, *et al.*, Phys. Lett. B **754**, 288–293 (2016).
[94] P. Zhang, *et al.*, Phys. Lett. B **767**, 20–24 (2017).
[95] Y. H. Zhang, *et al.*, Phys. Rev. C **98**, 014319 (2018).
[96] Y. M. Xing, *et al.*, Phys. Lett. B **781**, 358–363 (2018).
[97] P. Walker, *et al.*, Int. J. Mass Spectr. **349-350**, 247–254 (2013).
[98] J. Yang, *et al.*, Nucl. Instr. Meth. B **317**, 263–265 (2013).
[99] M. S. Sanjari, *et al.*, *Technical Design Report for the Schottky Detector System of ILIMA* (2018).
[100] M. S. Sanjari, Zenodo, **7615693**, (2023), https://zenodo.org/record/7615693
[101] D. Dmytriiev, *et al.*, J. Phys. Conf. Ser. 1668 **012014** (2020).